Electronic Supplementary Information for:

Ligand Design of Zero-Field Splitting in Trigonal Prismatic Ni(II) Cage Complexes

Anthony J. Campanella,[a] Tyler M. Ozvat,[a] and Joseph M. Zadrozny*[a]

[a]*Department of Chemistry, Colorado State University, Fort Collins, Colorado 80523, USA.*

Table of Contents

Full Experimental Details

General Considerations. Compounds **1**-**3** were synthesized using acetonitrile (MeCN) purified through a commercial solvent purification system from LC Technologies. Non-purified MeCN in atmospheric conditions was found to work as well for the syntheses of **1**-**3**, however, higher yields were obtained using MeCN from a solvent purification system under N_2. Nitromethane ($MeNO_2$) used in the synthesis of **4**-**5** was degassed via the freeze-pump-thaw method and stored over 3 Å molecular sieves for 3 days prior to use. Anhydrous nickelous chloride dimethoxyethane adduct ($NiCl_2$•DME) was synthesized following a literature procedure.[1] 3,4-hexanedione-dioxime,[2] glyoxime,[3] and dichloroglyoxime[3] were synthesized following their respective literature procedures. The aryl boronic acids used throughout were purchased from commercial sources and used as received. Prior to the synthesis of **4** and **5**, excess moisture was removed from phenylboronic acid by heating the powder at 80°C under high vacuum for 12 hours.

Ni(L1)•0.5H_2O (1) In a 25 mL round-bottom flask, 202 mg (0.85 mmol, 1 eq.) of $NiCl_2$•6H_2O was dissolved in 10 mL of MeCN, followed by 367 mg (2.55 mmol, 3 eq.) of 3,4-hexanedione-dioxime, producing a maroon solution. This solution was heated at reflux for one hour under N_2, followed by the addition of 360 mg (1.70 mmol, 2 eq.) of pentafluorophenylboronic acid. The subsequent solution was then refluxed for four days, while remaining under N_2. After this time, a light green precipitant was observable in the reaction flask. The solution was cooled to room temperature and filtered open to air. The resulting light green powder was washed with MeCN (3 × 5 mL) followed by ethyl ether (3 × 10 mL) and dried overnight in a vacuum oven at 70°C. The final yield was 310 mg (43%) of **1**. Crystals suitable for single crystal x-ray diffraction were grown by layering a saturated chloroform solution of **1** with MeCN. IR (cm^{-1}, diamond ATR): 2984, 2944, 2880, 1645, 1609, 1467, 1293, 1129, 1106, 1058, 1032, 978, 919, 821, 752, 587. UV-vis (Methylene chloride); λ_{max} (ε_M, $M^{-1}cm^{-1}$): 770 nm (41.8). LC-MS (m/z): positive ion mode: $\{H[Ni(L1)]\}^+$, 841.17. Elemental analysis for $C_{30}H_{40}B_2F_{10}N_6NiO_6$•0.5$H_2O$ calculated (found): %C: 42.40 (42.35), %H: 3.68 (3.97), %N: 9.89 (9.68).

Ni(L2)•1H_2O (2) In a 25 mL round-bottom flask, 178 mg (0.75 mmol, 1 eq.) of $NiCl_2$•6H_2O was dissolved in 10 mL of MeCN, followed by 324 mg (2.25 mmol, 3 eq.) of 3,4-hexanedione-dioxime, producing a maroon solution. This solution was heated at reflux for one hour under N_2, followed

by the addition of 273 mg (1.50 mmol, 2 eq.) of 3,5-dimethoxyphenylboronic acid. The subsequent solution was then refluxed for two days, while remaining under N_2. After this time, a light green precipitant was observable in the reaction flask. The solution was cooled to room temperature and filtered open to air. The resulting light green powder was washed with MeCN (3 × 5 mL) followed by ethyl ether (3 × 10 mL) and dried overnight in a vacuum oven at 70°C. The final yield was 415 mg (69%) of **2**. Crystals suitable for single crystal x-ray diffraction were grown by layering a saturated methylene chloride solution of **2** with MeCN IR (cm^{-1}, diamond ATR): 2978, 2946, 2932, 2832, 1583, 1456, 1410, 1331, 1284, 1245, 1198, 1171, 1148, 1106, 1062, 1025, 989, 900, 846, 816, 756, 710, 585. UV-vis (H_2O); λ_{max} (ε_M, $M^{-1}cm^{-1}$): 772 nm (62.3); 464 nm (94.5). LC-MS (m/z): positive ion mode: $\{H[Ni(L2)]\}^+$, 781.29. Elemental analysis for $C_{34}H_{48}B_2N_6NiO_{10}\bullet H_2O$ calculated (found): %C: 51.10 (50.87), %H: 6.31 (6.05), %N: 10.52 (10.98).

Ni(L3) (3) In a 25 mL round-bottom flask, 119 mg (0.5 mmol, 1 eq.) of $NiCl_2\bullet 6H_2O$ was dissolved in 10 mL of MeCN, followed by 216 mg (1.5 mmol, 3 eq.) of 3,4-hexanedione-dioxime, producing a maroon solution. This solution was heated at reflux for one hour under N_2, followed by the addition of 121 mg (1.0 mmol, 2 eq.) of phenylboronic acid. The subsequent solution was then refluxed for two days, while remaining under N_2. After this time, a light green precipitant was observable in the reaction flask. The solution was cooled to room temperature and filtered open to air. The resulting light green powder was washed with MeCN (3 × 5 mL) followed by ethyl ether (3 × 10 mL) and dried overnight in a vacuum oven at 70°C. The final yield was 281 mg (85%) of **3**. Crystals suitable for single crystal x-ray diffraction were grown by layering a saturated methylene chloride solution of **3** with ethyl ether. IR (cm^{-1}, diamond ATR): 2976, 2940, 2876, 1612, 1461, 1433, 1218, 1179, 1105, 1055, 1016, 950, 899, 816, 745, 705, 651, 577, 492. UV-vis (H_2O); λ_{max} (ε_M, $M^{-1}cm^{-1}$): 772 nm (55.5); LC-MS (m/z): positive ion mode: $\{H[Ni(L3)]\}^+$, 661.25. Elemental analysis for $C_{30}H_{40}B_2N_6NiO_6$ calculated (found): %C: 54.51 (54.19), %H: 6.10 (5.92), %N: 12.71 (12.63).

Ni(L4)•2.5H_2O (4) In a N_2 glove box, 200 mg (0.91 mmol, 1 eq.) of $NiCl_2$•DME was dissolved in 10 mL of $MeNO_2$ in a 25 mL Schlenk flask, followed by 241 mg (2.73 mmol, 3 eq.) of glyoxime, and 221 mg (1.82 mmol, 2 eq.) of phenylboronic acid. The reaction vessel was removed from the glovebox and affixed to a Schlenk line under N_2. The solution was heated at reflux for four days.

The solution was then cooled to room temperature and filtered open to air. The resulting light green powder was washed with MeOH (3 × 5 mL) followed by ethyl ether (3 × 10 mL) and dried overnight in a vacuum oven at 70°C. The final yield was 319 mg (65%) of **4**. Crystals suitable for single crystal x-ray diffraction were grown by vapor diffusion of ethyl ether into a saturated 1,4-dioxane solution of **4**. IR (cm^{-1}, diamond ATR): 3054, 3015, 2963, 2852, 1596, 1499, 1433, 1281, 1260, 1260, 1217, 1131, 1095, 943, 890, 847, 823, 754, 721, 700, 585. UV-vis (H_2O); λ_{max} (ε_M, $M^{-1}cm^{-1}$): 764 nm (29.2); LC-MS (m/z): positive ion mode: $\{H[Ni(L4)]\}^+$, 493.07. Elemental analysis for $C_{18}H_{16}B_2N_6NiO_6 \bullet 2.5H_2O$ calculated (found): %C: 40.21 (40.42), %H: 3.94 (3.55), %N: 15.63 (15.41).

Ni(L5) (5) In a N_2 glove box, 110 mg (0.5 mmol, 1 eq.) of $NiCl_2$•DME was dissolved in 10 mL of $MeNO_2$ in a 25 mL Schlenk flask, followed by 235 mg (1.5 mmol, 3 eq.) of dichloroglyoxime, and 122 mg (1.0 mmol, 2 eq.) of phenylboronic acid. The reaction vessel was removed from the glovebox and affixed to a Schlenk line under N_2. The solution was heated at reflux for two days. The solution was then cooled to room temperature and filtered open to air. The resulting light green powder was washed with MeOH (3 × 5 mL) followed by ethyl ether (3 × 10 mL) and dried overnight in a vacuum oven at 70°C. The final yield was 326 mg (93%) of **5**. Crystals suitable for single crystal x-ray diffraction were grown by vapor diffusion of ethyl ether into a saturated dichloromethane solution of **5**. IR (cm^{-1}, diamond ATR): 3074, 3054, 3014, 1562, 1433, 1260, 1224, 1148, 1081, 959, 910, 883, 946, 761, 704, 657, 532. UV-vis (H_2O); λ_{max} (ε_M, $M^{-1}cm^{-1}$): 838 nm (44.2). Elemental analysis for $C_{18}H_{10}B_2N_6NiO_6$ calculated (found): %C: 30.62 (30.67), %H: 1.44 (1.33), %N: 12.02 (11.79).

X-ray Data Collection, Structure Solution and Refinement for 1-5. The diffraction data were collected at the X-Ray Diffraction facility of the Analytical Resources Core at Colorado State University. Data for **1-5** were collected on a Bruker D8 Quest ECO single-crystal X-ray diffractometer equipped with Mo Kα (λ = 0.71073 A). Data were collected and integrated using Bruker Apex 3 software. Absorption correction were applied using SADABS.[4] Space group assignments were determined by examination of systematic absences, E7 statistics, and successive refinement of the structures. Crystal structures were solved using SHELXT and refined with the aid of successive difference Fourier maps by SHELXL operated in conjunction with OLEX2 software.[5–7] None of the crystals demonstrated decay by X-ray radiation over the course of the

experiment. Hydrogen atoms were placed in ideal positions and refined using a riding model for all structures. In **1**, two disordered carbon atoms in one of the ethyl side-arms were modeled with fixed occupancies of 0.50 and 0.50, and 0.67 and 0.33. Crystallographic information files for **1-5** are available in the CSD at accession numbers 2086087-2086091.

Magnetic Measurements. Magnetic data were collected on a Quantum Design MPMS SQUID magnetometer. Microcrystalline samples of **1-5** were pulverized and placed into a gelatin capsule then restrained with molten eicosane. Direct current (dc) measurements were obtained with 1000, 5000, 10000, and 30000 G applied fields with temperatures ranging from 1.8 to 300 K. All dc measurements were corrected for the diamagnetic contribution of the sample holder, as well as the restraining material and ligand framework (calculated using Pascal's constants).[8]

Computational Details. All computations were carried out using Orca 4.11 software package.[9] Experimental single crystal X-ray diffraction structures were used as the starting geometries for all computations with all C–H bonds modified to 1.09 Å. Initial orbital energies were generated via DFT (B3LYP functional)[10] using the SVP basis set,[11] RIJCOSX approximation,[12,13] and unrestricted natural orbitals (UNOs). With respects to the five 3d-orbitals and eight electrons of nickel(II), complete active space self-consistent field (CASSCF)[14,15] calculations were performed with the UNOs to yield zero-field splitting parameters, including D and g_{iso}. The %CASSCF block included triplet and singlet multiplets with 10 and 15 excitations, respectively. Additionally, calculations were completed including relativistic effects, spin-orbit coupling, and spin-spin coupling, and convergence followed using the SOSCF switchstep. Ab initio ligand field theory calculations (AILFT)[16,17] were complete starting from successfully converged CASSCF outputs via MOREAD function and included NEVPT2[18–20] treatment.

Electron Paramagnetic Resonance. EPR spectra collected herein were simulated using Easyspin[21] with the function Pepper (frozen solution and solid powder) and were refined using simulations of the experimental data. All samples were prepared at atmospheric conditions as 5 mM solutions in a glassing mixture of chloroform and toluene (1:1 v/v) the same day the measurements took place. X-band CW EPR data were collected on a Bruker ESR-300 spectrometer equipped with a ColdEdge liquid helium cryostat and the Bruker ER 4116DM dual-

mode resonator. No signal that could be attributed to any of the nickel complexes studied was found under these conditions.

Other Physical Measurements. Elemental analyses were performed by Roberson Microlit Laboratories (Ledgewood, New Jersey, USA). Infrared spectra were recorded on a Nicolet 6700 FTIR spectrometer using a diamond window ATR. Electronic absorption spectra of all complexes were recorded on aqueous with a Hewlett-Packard 8453 spectrophotometer using standard quartz cuvettes with a 1 cm path length. Mass spectral analyses were performed on an Agilent 6224 Accurate Mass TOF LC/MS in positive ion mode using direct injection. Peak assignment was on the basis of m/z, interpeak spacing, and isotopic distribution.

Table S1. Crystallographic information for the structural refinement of **1**.

Empirical formula	$C_{30}H_{30}B_2F_{10}N_6NiO_6$
Formula weight	840.96 g/mol
Temperature	104.13 K
Crystal system	Triclinic
Space group	P-1
a	11.7082(3) Å
b	12.2248(3) Å
c	13.9254(4) Å
α	67.6230(10)°
β	88.3260(10)°
γ	71.7290(10)°
Volume	1740.90(8) $Å^3$
Z	2
ρ_{calc}	1.604 g cm^{-3}
μ	0.663 mm^{-1}
F(000)	856.0
Crystal color	Green
Crystal size	0.138 × 0.061 × 0.031 mm^3
Radiation	MoKα (λ = 0.71073 Å)
2θ range for data collection	3.18 to 52.74°
Index ranges	$-14 \leq h \leq 14$, $-15 \leq k \leq 15$, $-17 \leq l \leq 17$
Reflections collected	96824
Independent collections	7132 [R_{int} = 0.0783, R_{sigma} = 0.0276]
Data/restraints/parameters	7132/0/501
Goodness-of-fit on F^2	1.134
Final R indexes [$I \geq 2\sigma$ (I)]	R_1 = 0.0431, wR_2 = 0.1100
Final R indexes [all data]	R_1 = 0.0576, wR_2 = 0. 0.1261
Largest diff. peak/hole	1.74/-0.67 e $Å^{-3}$

Table S2. Crystallographic information for the structural refinement of **2**.

Empirical formula	$C_{34}H_{46}B_2N_6NiO_{10}$
Formula weight	779.10 g/mol
Temperature	100.01 K
Crystal system	Monoclinic
Space group	C2/c
a	26.8983(12) Å
b	8.7226(4) Å
c	17.7343(7) Å
α	90°
β	117.800(2)°
γ	90°
Volume	3680.6(3) Å^3
Z	4
ρ_{calc}	1.406 g cm^{-3}
μ	0.592 mm^{-1}
F(000)	1640.0
Crystal color	Green
Crystal size	0.268 × 0.127 × 0.029 mm^3
Radiation	MoKα (λ = 0.71073 Å)
2θ range for data collection	3.424 to 49.418°
Index ranges	$-31 \leq h \leq 31$, $-10 \leq k \leq 10$, $-20 \leq l \leq 20$
Reflections collected	45379
Independent collections	3142 [R_{int} = 0.1308, R_{sigma} = 0.0424]
Data/restraints/parameters	3142/0/245
Goodness-of-fit on F^2	1.109
Final R indexes [$I \geq 2\sigma$ (I)]	R_1 = 0.0673, wR_2 = 0.1695
Final R indexes [all data]	R_1 = 0.0899, wR_2 = 0.1899
Largest diff. peak/hole	1.55/-0.84 e Å^{-3}

Table S3. Crystallographic information for the structural refinement of **3**.

Empirical formula	$C_{31}H_{42}B_2Cl_2N_6NiO_6$
Formula weight	745.92 g/mol
Temperature	100.02 K
Crystal system	Triclinic
Space group	P1
a	8.7045(3) Å
b	12.6193(5) Å
c	16.8514(6) Å
α	108.029(2)°
β	91.507(2)°
γ	100.848(2)°
Volume	1721.60(11) $Å^3$
Z	2
ρ_{calc}	1.439 g cm^{-3}
μ	0.771 mm^{-1}
F(000)	780.0
Crystal color	Green
Crystal size	0.256 × 0.043 × 0.037 mm^3
Radiation	MoKα (λ = 0.71073 Å)
2θ range for data collection	3.468 to 52.742°
Index ranges	$-10 \leq h \leq 10$, $-15 \leq k \leq 15$, $-21 \leq l \leq 21$
Reflections collected	49643
Independent collections	14052 [R_{int} = 0.0612, R_{sigma} = 0.0586]
Data/restraints/parameters	14052/3/877
Goodness-of-fit on F^2	1.098
Final R indexes [$I \geq 2\sigma$ (I)]	R_1 = 0.0408, wR_2 = 0.0908
Final R indexes [all data]	R_1 = 0.0565, wR_2 = 0.1049
Largest diff. peak/hole	0.44/-0.57 e $Å^{-3}$
Flack parameter	0.387(6)

Table S4. Crystallographic information for the structural refinement of **4**.

Empirical formula	$C_{18}H_{16}B_2N_6NiO_6$
Formula weight	492.68 g/mol
Temperature	214.44 K
Crystal system	Monoclinic
Space group	$P2_1/c$
a	11.291(6) Å
b	11.251(4) Å
c	15.826(6) Å
α	90°
β	104.49(2)°
γ	90°
Volume	1946.5(15) $Å^3$
Z	4
ρ_{calc}	1.681g cm^{-3}
μ	1.051 mm^{-1}
F(000)	1008.0
Crystal color	Green
Crystal size	0.102 × 0.065 × 0.032 mm^3
Radiation	MoKα (λ = 0.71073 Å)
2θ range for data collection	3.726 to 52.04°
Index ranges	$-13 \leq h \leq 13$, $-13 \leq k \leq 13$, $-19 \leq l \leq 19$
Reflections collected	74743
Independent collections	3824 [R_{int} = 0.0838, R_{sigma} = 0.0247]
Data/restraints/parameters	3824/0/298
Goodness-of-fit on F^2	1.222
Final R indexes [$I \geq 2\sigma$ (I)]	R_1 = 0.0306, wR_2 = 0.0813
Final R indexes [all data]	R_1 = 0.0442, wR_2 = 0.0995
Largest diff. peak/hole	0.61/-0.60 e $Å^{-3}$

Table S5. Crystallographic information for the structural refinement of **5**.

Empirical formula	$C_{18}H_{10}B_2Cl_6N_6NiO_6$
Formula weight	699.35 g/mol
Temperature	110.22 K
Crystal system	Triclinic
Space group	P-1
a	8.1747(10) Å
b	12.442(2) Å
c	13.2849(18) Å
α	96.637(7)°
β	103.105(9)°
γ	108.640(7)°
Volume	1220.8(3) $Å^3$
Z	2
ρ_{calc}	1.903 g cm^{-3}
μ	1.503 mm^{-1}
F(000)	696.0
Crystal color	Green
Crystal size	0.052 × 0.046 × 0.035 mm^3
Radiation	MoKα (λ = 0.71073 Å)
2θ range for data collection	3.216 to 52.988°
Index ranges	$-10 \leq h \leq 10$, $-15 \leq k \leq 15$, $-16 \leq l \leq 16$
Reflections collected	52346
Independent collections	5031 [R_{int} = 0.1056, R_{sigma} = 0.0477]
Data/restraints/parameters	5031/0/352
Goodness-of-fit on F^2	1.044
Final R indexes [$I \geq 2\sigma$ (I)]	R_1 = 0.0428, wR_2 = 0.0957
Final R indexes [all data]	R_1 = 0.0649, wR_2 = 0.1043
Largest diff. peak/hole	1.24/-0.40 e $Å^{-3}$

Table S6. Contributions to *D* respective of triplet (*T*) and singlet (*S*) excited states in each complex and their respective energies.

	1		2		3		4		5	
State	Contrib. to *D* (cm^{-1})	ΔE (cm^{-1})	Contrib. to *D* (cm^{-1})	ΔE (cm^{-1})	Contrib. to *D* (cm^{-1})	ΔE (cm^{-1})	Contrib. to *D* (cm^{-1})	ΔE (cm^{-1})	Contrib. to *D* (cm^{-1})	ΔE (cm^{-1})
T1	-7.38	11168.9	-1.94	10532.7	-12.12	11379.4	-11.96	11446.1	-6.49	10310.1
T2	18.84	12159.4	1.99	10829.0	18.17	12366.0	21.11	12227.3	19.69	10888.1
T3	17.54	12425.4	23.24	11584.8	19.63	12493.8	20.53	12326.7	19.33	11541.6
T4	3.17	12613.6	22.40	11620.7	0.66	13371	0.10	13062.2	5.89	11572.5
S2	-5.27	24777.8	-5.04	23927.6	-5.13	25323.2	-5.44	25081.5	-5.48	24368.1
S3	-5.10	25247.5	-4.96	24148.4	-5.32	25705.1	-5.37	25616.6	-5.02	24275.3
S4	16.73	25383.1	19.01	24151.3	15.30	25824.7	16.17	25670.4	17.41	24407.3

Table S7. Multiconfiguration coefficients for **1**.[a]

Excitation Configurations of **1**

T1		***T2***		***T3***		***T4***		***S2***		***S3***		***S4***	
A	*config.*	*A*	*config.*	*A*	*config.*	*A*	*config.*	*A*	*config.*	*A*	*config.*	*A*	*config.*
0.226	22211	0.614	12122	0.455	21212	0.476	22121	0.382	12122	0.139	22220	0.250	22211
0.153	22121	0.103	21212	0.159	11222	0.211	22211	0.160	22211	0.133	22022	0.172	22022
0.144	12212	0.088	12221	0.144	22121	0.105	12221	0.121	11222	0.125	21212	0.107	22121
0.139	21221	0.066	22111	0.109	12212	0.062	12122	0.111	22202	0.124	22121	0.101	12212
0.117	12122	0.055	11222	0.080	21221	0.057	11222	0.069	21221	0.098	12212	0.090	11222
0.100	22112	0.038	12212	0.024	12221	0.033	21122	0.054	22220	0.081	20222	0.074	21122
0.063	21212	0.024	22211	0.019	22112	0.020	12212	0.039	22121	0.075	02222	0.069	22202
0.052	21122	0.008	22121	0.009	22211	0.019	21221	0.036	21212	0.065	22112	0.037	12221
0.004	12221					0.015	21212	0.010	12221	0.059	21221	0.032	02222
								0.007	20222	0.055	12122	0.020	12122
								0.005	12212	0.024	12221	0.014	21212
								0.004	22112	0.011	21122	0.014	22220
										0.007	22211	0.011	22112
										0.004	11222	0.007	21221

[a.] Configurations here are listed as occupancy of *d* orbitals, with increasing energy from left to right. For example, in the *T1* column above, "22211" indicates a configuration of $(d_{z2})^2(d_{x2-y2})^2(d_{xy})^2(d_{xz})^1(d_{yz})^1$, like depicted in Fig. 3c of the main text, and the "A" number of 0.226 indicates the contribution of that configuration to the *T1* state.

Table S8. Multiconfiguration coefficients for **2**.

Excitation Configurations of **2**

T1		*T2*		*T3*		*T4*		*S2*		*S3*		*S4*	
A	*config.*	*A*	*config.*	*A*	*config.*	*A*	*config.*	*A*	*config.*	*A*	*config.*	*A*	*config.*
0.352	12122	0.436	11222	0.476	21212	0.451	21221	0.554	11222	0.200	02222	0.324	21212
0.340	21212	0.198	22112	0.273	22121	0.275	12212	0.352	22211	0.178	20222	0.217	12221
0.247	12221	0.183	22211	0.249	12122	0.224	11222	0.073	22112	0.149	22022	0.213	12122
0.061	22121	0.104	12212			0.020	22112	0.014	21221	0.133	22202	0.176	20222
		0.054	21221			0.019	22211	0.007	12212	0.123	22121	0.041	22202
		0.025	21122			0.011	21122			0.109	21212	0.024	22220
										0.084	12221	0.004	22121
										0.023	12122		

[a.] Configurations here are listed as occupancy of *d* orbitals, with increasing energy from left to right. For example, at the top of the *T1* column above, "12122" indicates a configuration of $(d_{z2})^1(d_{x2-y2})^2(d_{xy})^1(d_{xz})^2(d_{yz})^2$, and the "A" number of 0.352 indicates the contribution of that configuration to the *T1* state.

Table S9. Multiconfiguration Coefficients for **3**.

Excitation Configurations of **3**

T1		*T2*		*T3*		*T4*		*S2*		*S3*		*S4*	
A	*config.*	*A*	*config.*	*A*	*config.*	*A*	*config.*	*A*	*config.*	*A*	*config.*	*A*	*config.*
0.550	21221	0.435	21212	0.531	12122	0.408	22121	0.146	12122	0.186	21212	0.373	21221
0.193	12122	0.245	12122	0.182	21221	0.234	12221	0.134	21221	0.143	12122	0.340	12122
0.136	12212	0.172	12221	0.149	21212	0.098	22211	0.131	21212	0.113	12221	0.100	02222
0.041	11222	0.086	22211	0.050	22211	0.088	11222	0.125	22121	0.107	22121	0.081	12212
0.036	22121	0.034	21122	0.030	12221	0.075	21122	0.110	22220	0.095	11222	0.063	20222
0.028	12221	0.014	21221	0.024	21122	0.068	21221	0.097	12221	0.086	22220	0.020	22112
0.007	21212	0.013	22112	0.018	12212	0.015	12212	0.068	02222	0.078	22211	0.012	22220
0.006	22112			0.010	22112	0.010	21212	0.059	22022	0.076	21221	0.003	12221
				0.005	22121			0.054	20222	0.043	22022		
								0.036	22211	0.025	22112		
								0.015	22112	0.017	21122		
								0.011	11222	0.013	02222		
								0.009	21122	0.011	20222		
								0.004	22202	0.007	22202		
								0.003	12212				

[a.] Configurations here are listed as occupancy of *d* orbitals, with increasing energy from left to right. For example, at the top of the *T1* column above, "21221" indicates a configuration of $(d_{z2})^2(d_{x2-y2})^1(d_{xy})^2(d_{xz})^2(d_{yz})^1$ and the "A" number of 0.550 indicates the contribution of that configuration to the *T1* state.

Table S10. Multiconfiguration coefficients for **4**.[a]

Excitation Configurations of **4**

T1		*T2*		*T3*		*T4*		*S2*		*S3*		*S4*	
A	*config.*	*A*	*config.*	*A*	*config.*	*A*	*config.*	*A*	*config.*	*A*	*config.*	*A*	*config.*
0.277	21212	0.415	12122	0.372	22211	0.374	22112	0.234	12122	0.320	21221	0.365	21212
0.236	12122	0.227	21212	0.281	11222	0.225	21212	0.216	22202	0.258	22112	0.161	22121
0.165	22112	0.119	12221	0.104	21122	0.143	12212	0.131	21222	0.200	12212	0.132	02222
0.113	11222	0.092	22211	0.062	22121	0.095	22121	0.078	22112	0.064	11222	0.103	12122
0.107	21221	0.040	22121	0.055	21221	0.089	11222	0.071	22022	0.047	22022	0.055	22202
0.069	22121	0.040	22112	0.051	12221	0.024	21122	0.068	22121	0.026	22202	0.052	22112
0.024	12221	0.032	12212	0.043	22112	0.021	21221	0.057	02222	0.024	22211	0.039	11222
0.005	22211	0.022	21122	0.026	21212	0.016	12221	0.041	11222	0.015	21212	0.034	12221
0.003	12212	0.007	21221	0.003	12212	0.015	12122	0.035	22211	0.015	12122	0.028	22022
		0.007	11222					0.034	12212	0.010	02222	0.010	20222
								0.012	21221	0.010	12221	0.007	21122
								0.009	12221	0.007	21122	0.005	22211
								0.009	21212	0.003	20222	0.004	12212
								0.005	22220			0.004	22220

[a.] Configurations here are listed as occupancy of *d* orbitals, with increasing energy from left to right. For example, at the top of the *T1* column above, "21212" indicates a configuration of $(d_{z2})^2(d_{x2-y2})^1(d_{xy})^2(d_{xz})^1(d_{yz})^2$ and the "A" number of 0.277 indicates the contribution of that configuration to the *T1* state.

Table S11. Multiconfiguration coefficients for **5**.[a]

Excitation Configurations of **5**

T1		*T2*		*T3*		*T4*		*S2*		*S3*		*S4*	
A	*config.*	*A*	*config.*	*A*	*config.*	*A*	*config.*	*A*	*config.*	*A*	*config.*	*A*	*config.*
0.681	21221	0.606	22121	0.504	22112	0.689	21212	0.381	22121	0.430	21221	0.378	22202
0.272	22112	0.269	12221	0.289	12212	0.099	22121	0.337	21212	0.347	22112	0.251	22220
0.023	12212	0.055	22211	0.097	21221	0.084	12221	0.107	22211	0.100	12212	0.165	22022
0.016	11222	0.039	21212	0.046	21212	0.079	22211	0.101	12221	0.050	22220	0.159	20222
0.003	22211	0.023	12122	0.024	12122	0.019	22112	0.026	11222	0.028	22202	0.012	21212
0.003	21212	0.003	21221	0.013	22121	0.012	12212	0.011	21122	0.012	12122	0.009	21221
		0.003	21122	0.009	22211	0.010	21221	0.010	22112	0.007	22022	0.009	22121
				0.008	21122	0.004	12122	0.006	20222	0.007	22121	0.008	12212
				0.008	11222	0.003	11222	0.005	12212	0.006	11222	0.004	02222
				0.004	12221			0.004	21221	0.005	20222	0.004	22112
								0.004	02222	0.005	22211		
								0.003	22022	0.003	21212		
								0.003	12122				

[a.] Configurations here are listed as occupancy of *d* orbitals, with increasing energy from left to right. For example, in the *T1* column above, "21221" indicates a configuration of $(d_{z2})^2(d_{x2-y2})^1(d_{xy})^2(d_{xz})^2(d_{yz})^1$ and the "A" number of 0.681 indicates the contribution of that configuration to the *T1* state.

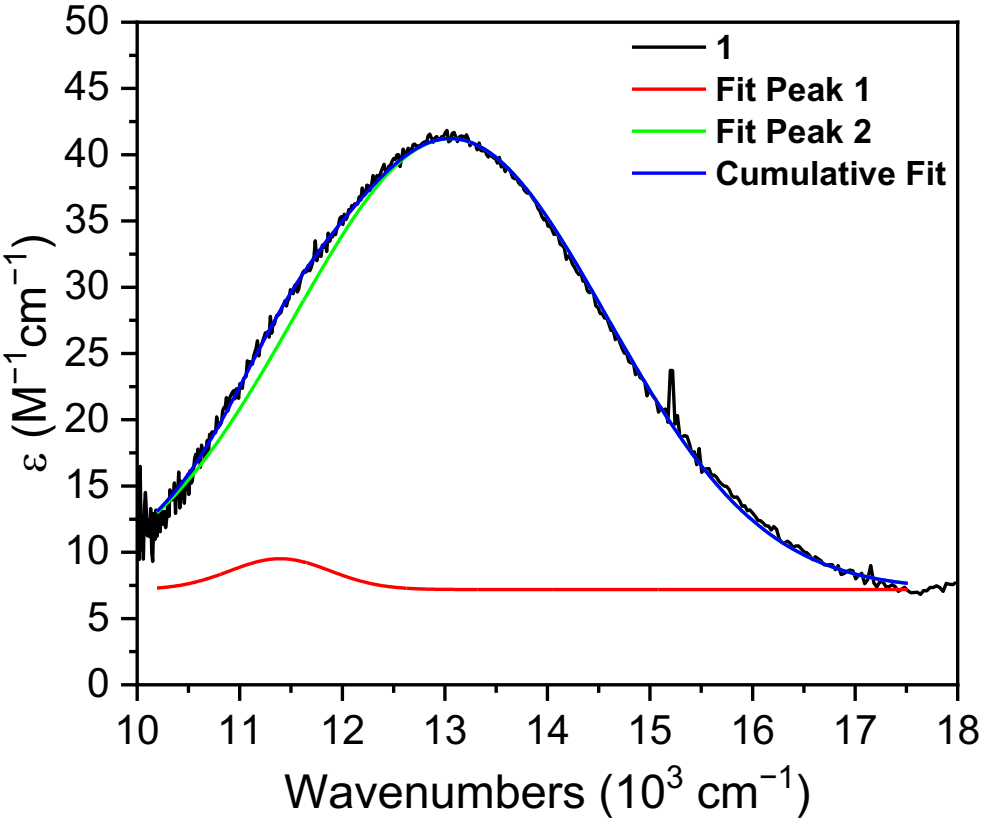

Figure S1. Deconvoluted electronic absorption spectra of **1**. Peak 1: 11406 cm^{-1}. Peak 2: 13071 cm^{-1}.

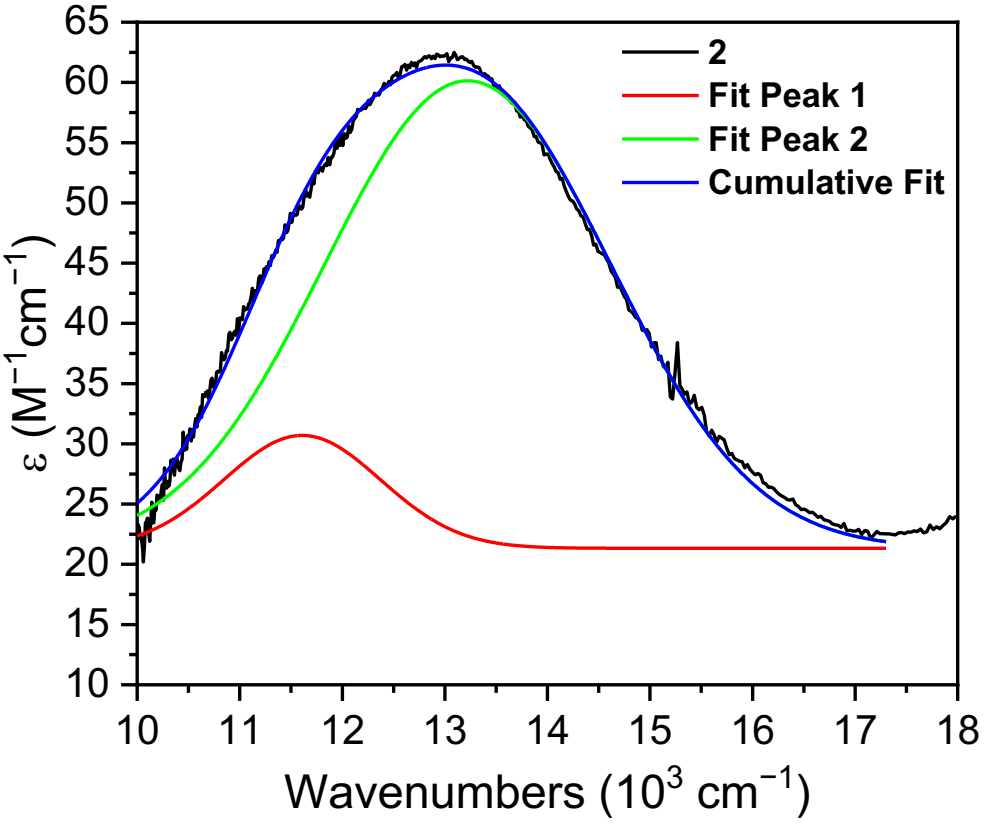

Figure S2. Deconvoluted electronic absorption spectra of **1**. Peak 1: 11397 cm^{-1}. Peak 2: 13053 cm^{-1}.

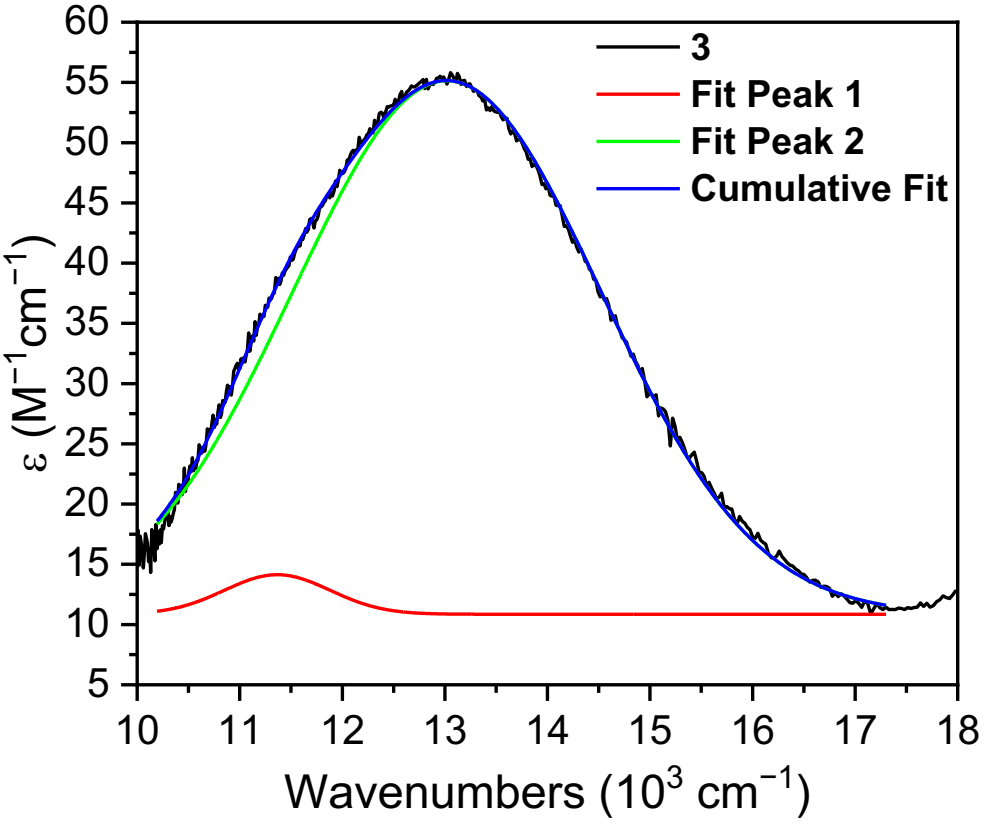

Figure S3. Deconvoluted electronic absorption spectra of **1**. Peak 1: 11608 cm^{-1}. Peak 2: 13222 cm^{-1}.

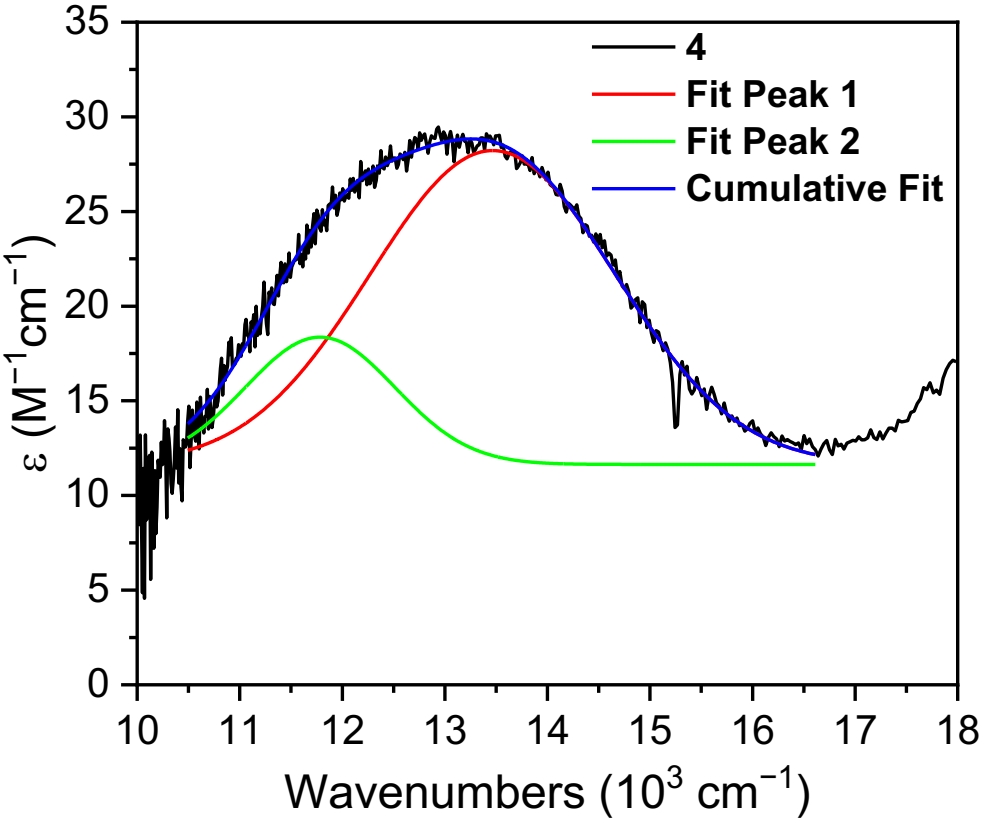

Figure S4. Deconvoluted electronic absorption spectra of **1**. Peak 1: 13412 cm^{-1}. Peak 2: 11703 cm^{-1}.

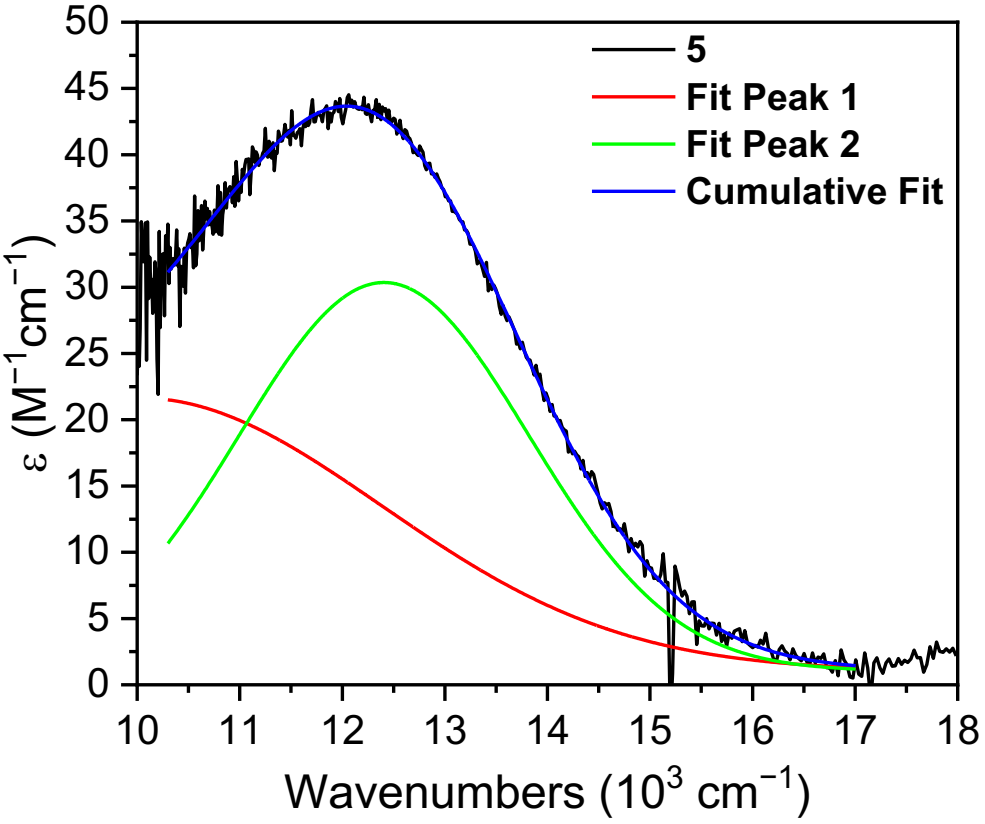

Figure S5. Deconvoluted UV-vis spectra of **1**. Peak 1: 9903 cm^{-1}. Peak 2: 12396 cm^{-1}.

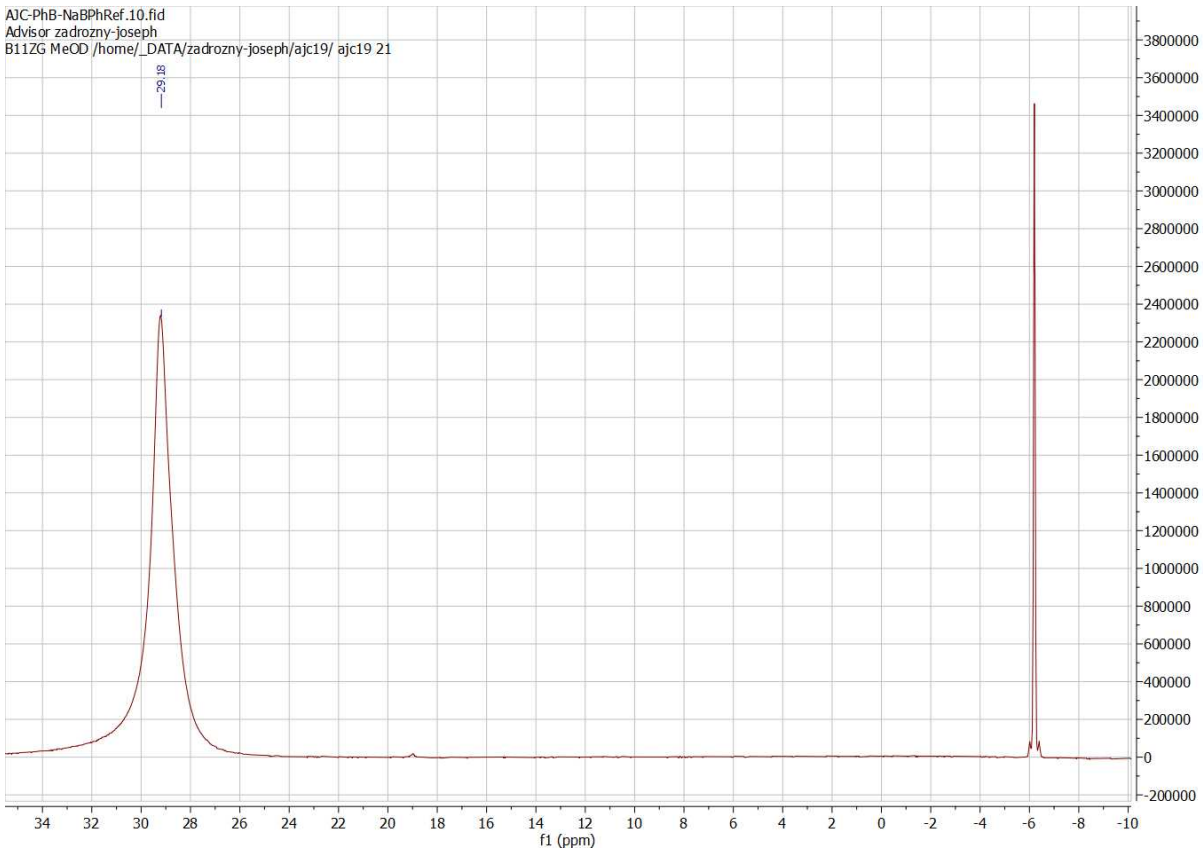

Figure S6. ^{11}B NMR spectra of phenylboronic acid referenced to $NaBPh_4$ collected in MeOH-d_4.

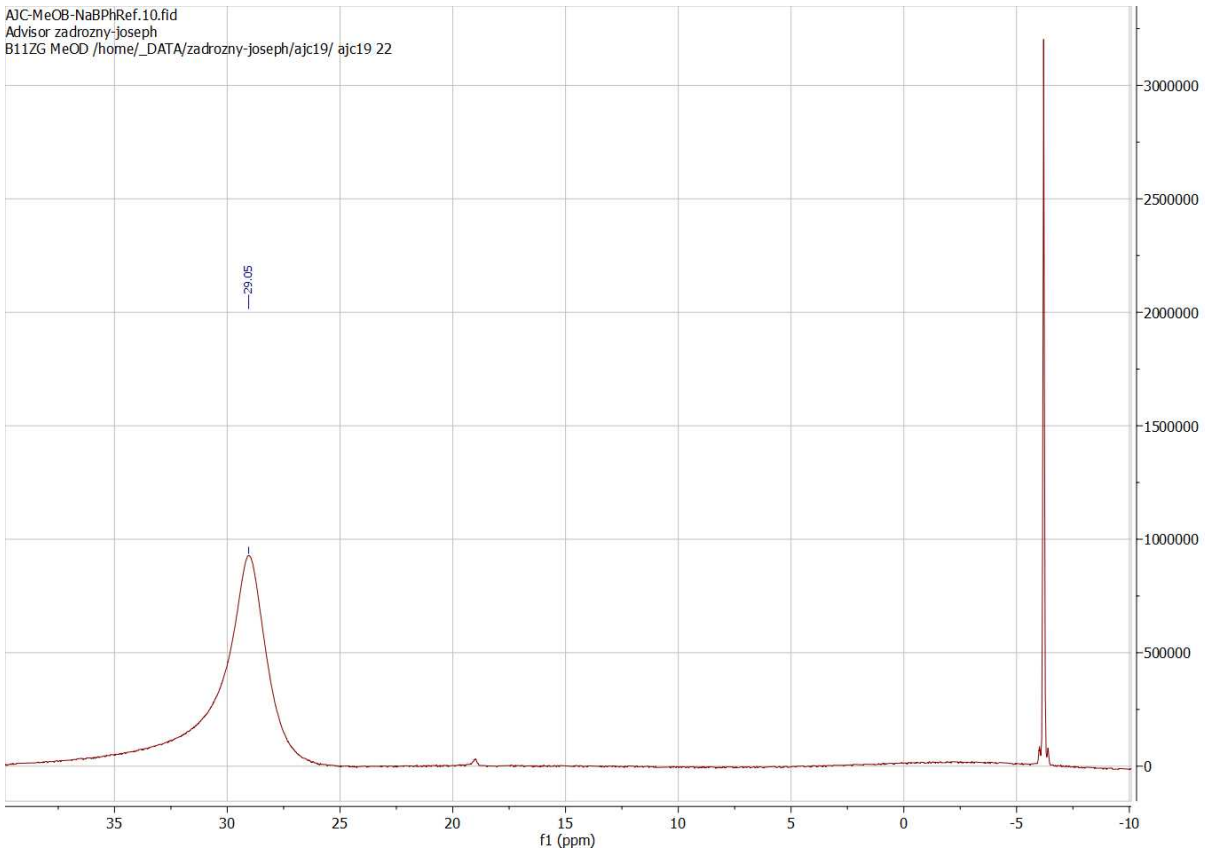

Figure S7. ^{11}B NMR spectra of 3,5-dimethoxyphenylboronic acid referenced to $NaBPh_4$ collected in MeOH-d_4.

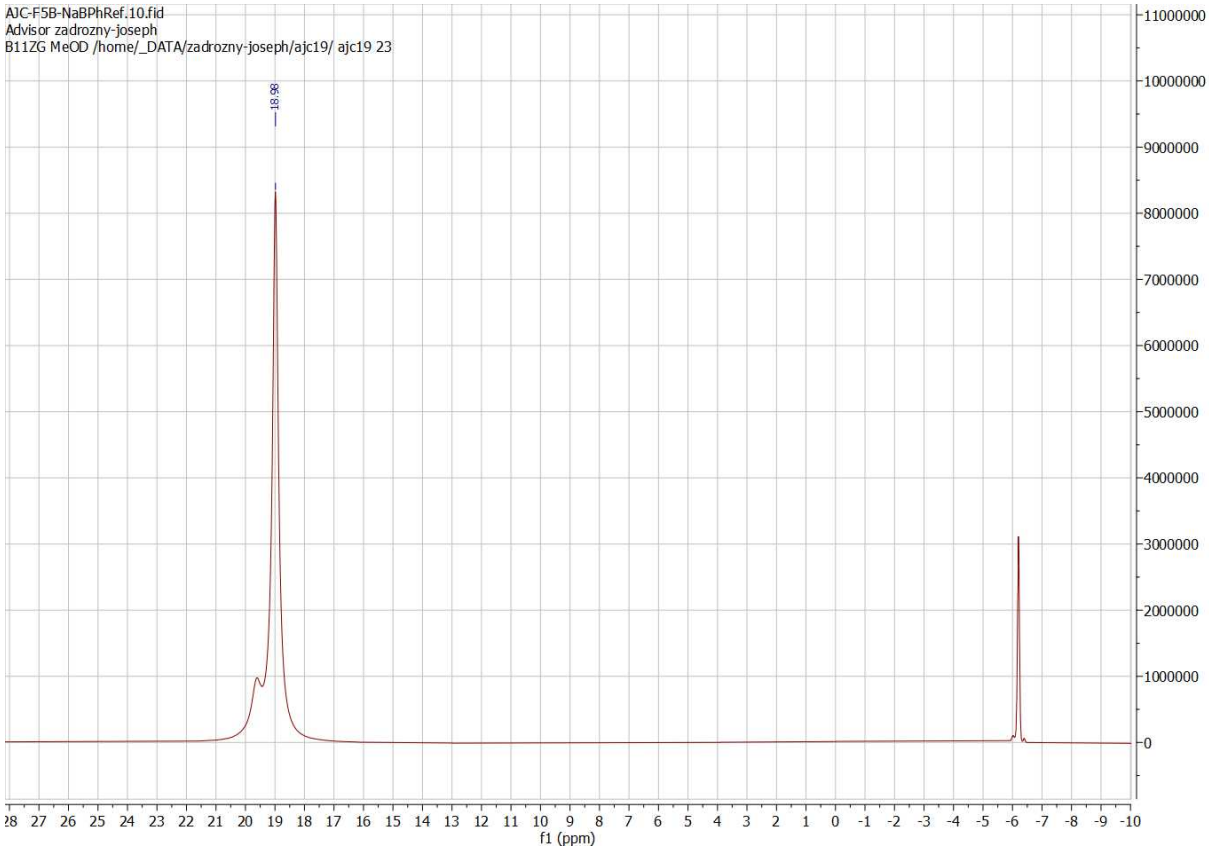

Figure S8. ^{11}B NMR spectra of pentafluorophenylboronic acid referenced to $NaBPh_4$ collected in MeOH-d_4.

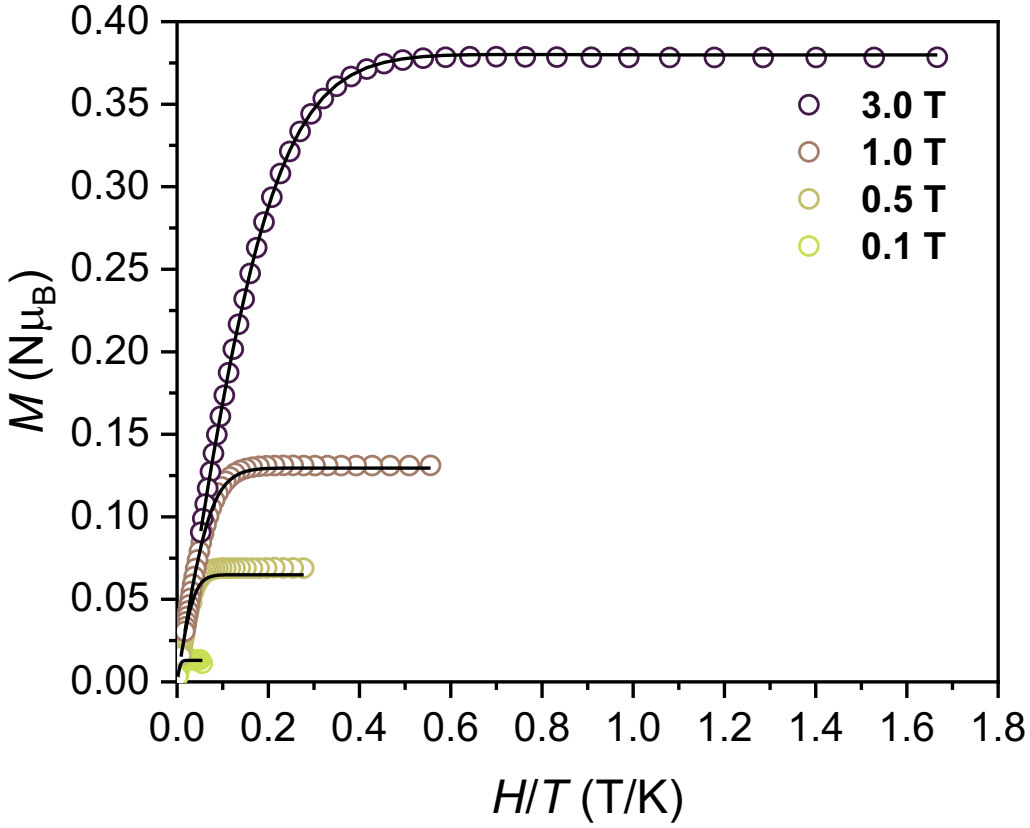

Figure S9. Reduced magnetization data and fits obtained through PHI for complex **1**.

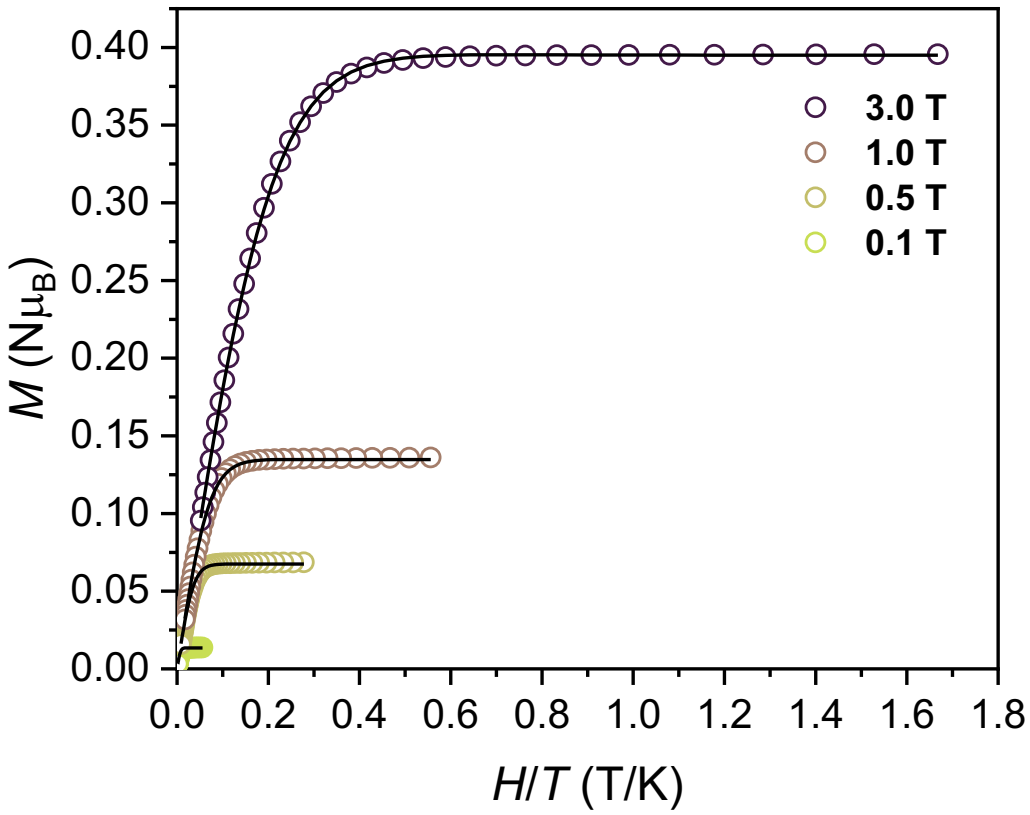

Figure S10. Reduced magnetization data and fits obtained through PHI for complex **2**.

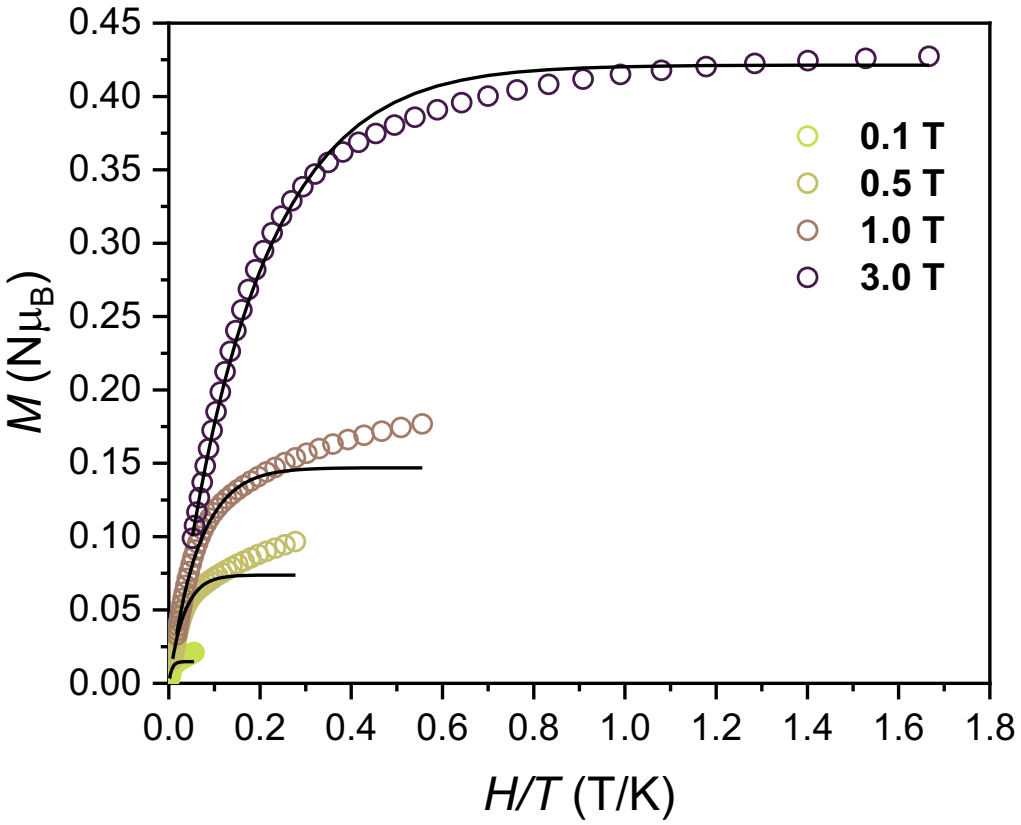

Figure S11. Reduced magnetization data and fits obtained through PHI for complex **4**.

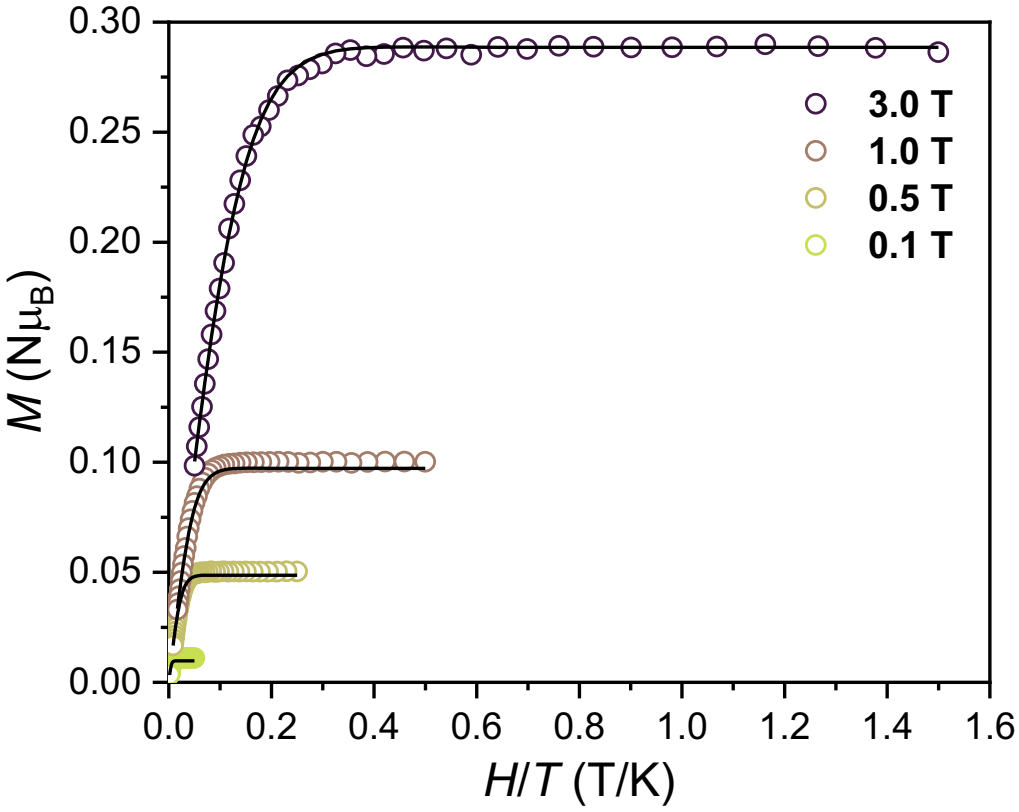

Figure S12. Reduced magnetization data and fits obtained through PHI for complex **5**.

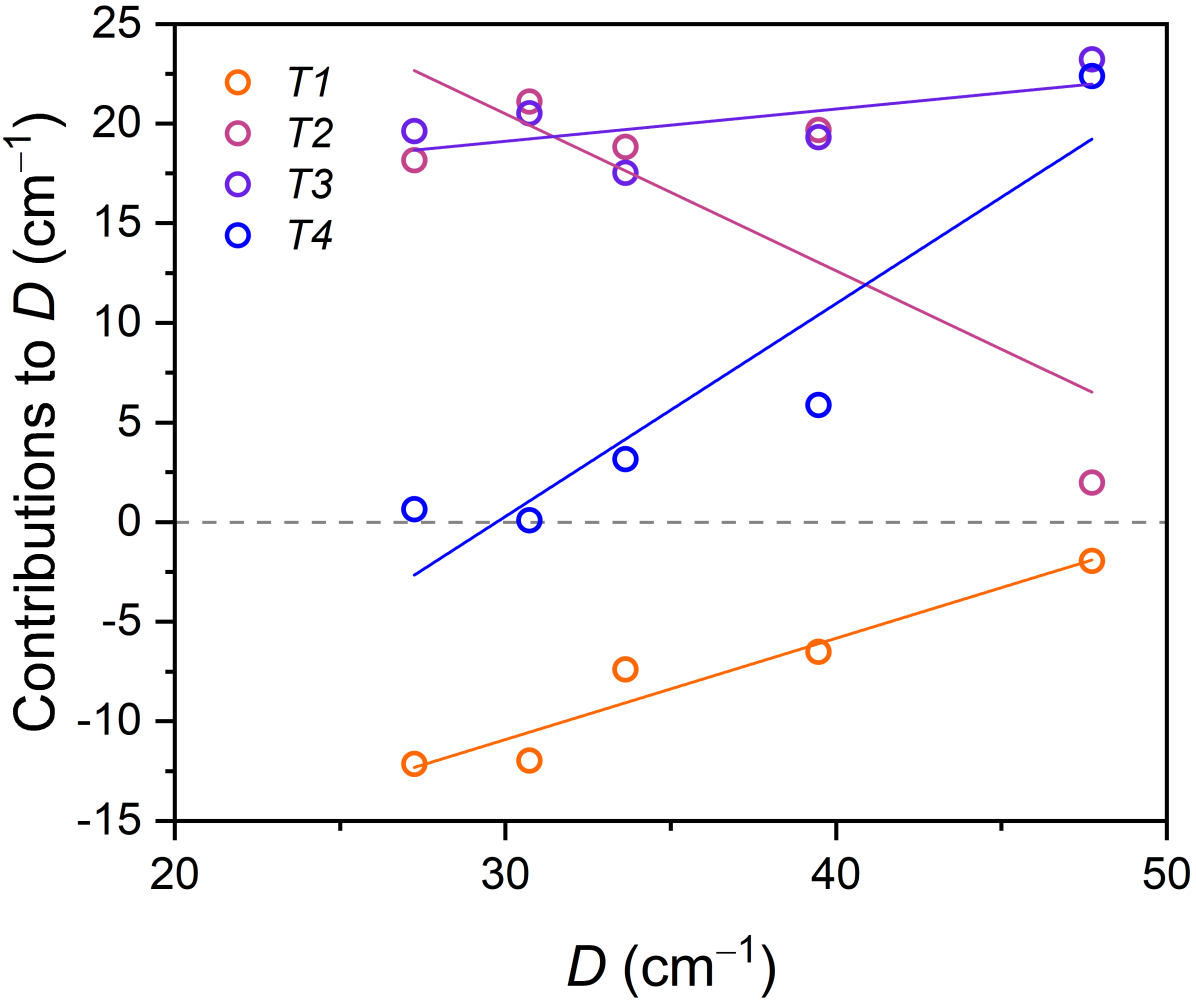

Figure S13. Contributions to *D* respective of triplet (*T*) excited states relative to the predicted total *D* value for each of the five compounds.

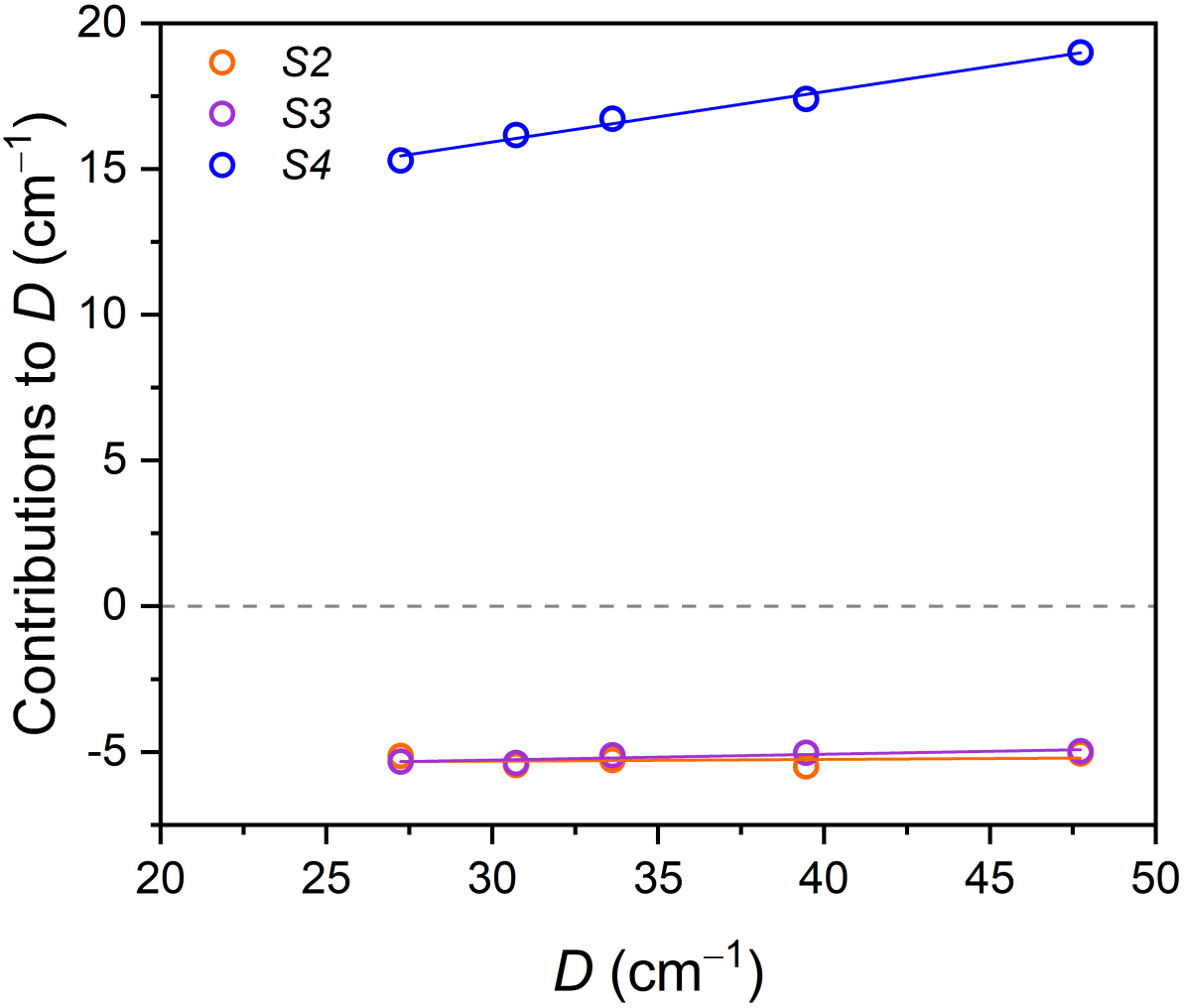

Figure S14. Contributions to *D* respective of singlet (*S*) excited states relative to the predicted total *D* value for each of the five compounds.

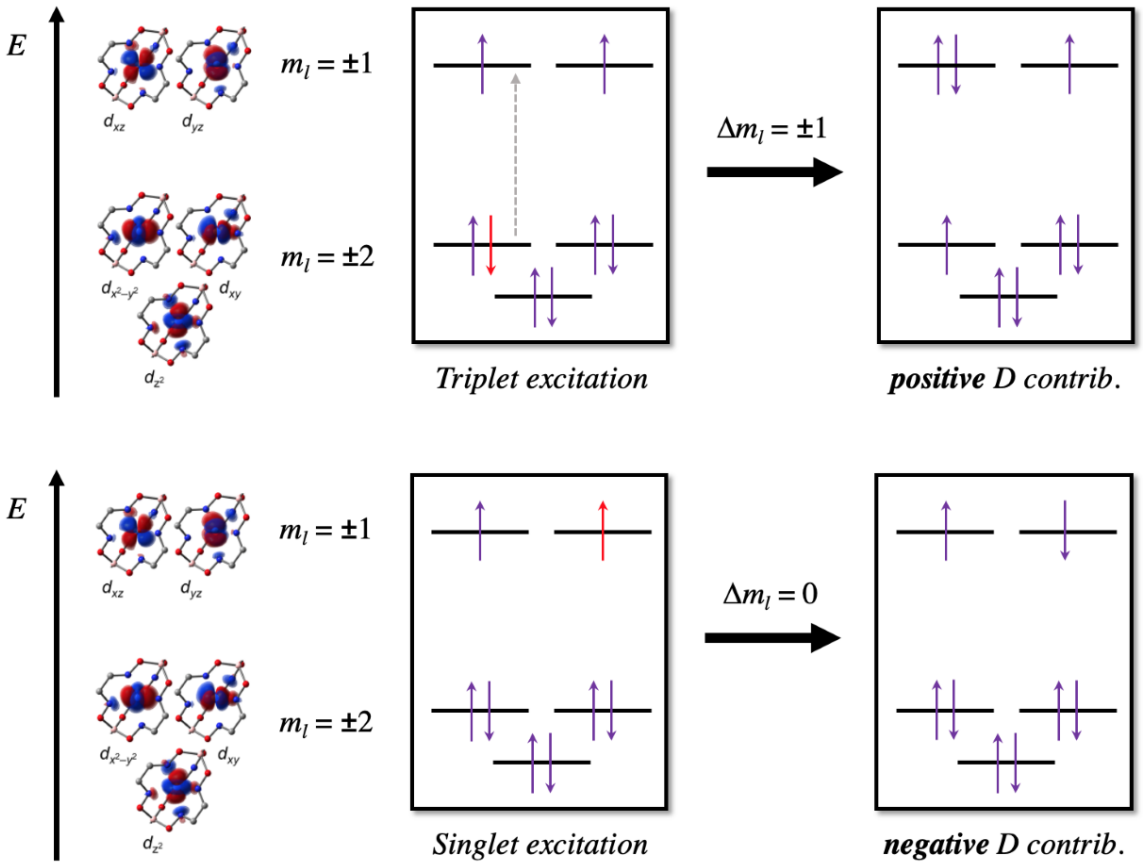

Figure S15. Depiction of some example triplet (top) and singlet (bottom) excitations responsible for positive and negative contributions to *D*, highlighted by the change in Δm_l for the specific excitation.

References

(1) Fowles, G. W. A.; Rice, D. A.; Walton, R. A. The Donor Properties of Simple Ethers—II[1]: Complexes of Manganese(II), Iron(II), Cobalt(II) and Nickel(II) Halides with Tetrahydrofuran and 1,2-Dimethoxyethane. *J. Inorg. Nucl. Chem.* **1969**, *31* (10), 3119–3131.

(2) Zaitsev, A. B.; Schmidt, E. Yu.; Vasil'tsov, A. M.; Mikhaleva, A. I.; Petrova, O. V.; Afonin, A. V.; Zorina, N. V. 1,2-Dioximes in the Trofimov Reaction. *Chem. Heterocycl. Compd.* **2006**, *42* (1), 34–41.

(3) Matsubara, R.; Ando, A.; Hasebe, H.; Kim, H.; Tsuneda, T.; Hayashi, M. Synthesis and Synthetic Application of Chloro- and Bromofuroxans. *J. Org. Chem.* **2020**, *85* (9), 5959–5972.

(4) Sheldrick, G. M. Program for Empirical Absorption Correction of Area Detector Data. *SADABS* **1996**.

(5) Sheldrick, G. M. SHELXT – Integrated Space-Group and Crystal-Structure Determination. *Acta Crystallogr. Sect. Found. Adv.* **2015**, *71* (1), 3–8.

(6) Sheldrick, G. M. Crystal Structure Refinement with SHELXL. *Acta Crystallogr. Sect. C Struct. Chem.* **2015**, *71* (1), 3–8.

(7) Sheldrick, G. M. A Short History of SHELX. *Acta Crystallogr. A* **2008**, *64* (Pt 1), 112–122.

(8) Bain, G. A.; Berry, J. F. Diamagnetic Corrections and Pascal's Constants. *J. Chem. Educ.* **2008**, *85* (4), 532.

(9) Neese, F. The ORCA Program System. *WIREs Comput. Mol. Sci.* **2012**, *2* (1), 73–78.

(10) Neese, F. A Spectroscopy Oriented Configuration Interaction Procedure. *J. Chem. Phys.* **2003**, *119* (18), 9428–9443.

(11) Schäfer, A.; Horn, H.; Ahlrichs, R. Fully Optimized Contracted Gaussian Basis Sets for Atoms Li to Kr. *J. Chem. Phys.* **1992**, *97* (4), 2571–2577.

(12) Neese, F.; Wennmohs, F.; Hansen, A.; Becker, U. Efficient, Approximate and Parallel Hartree-Fock and Hybrid DFT Calculations. A 'Chain-of-Spheres' Algorithm for the Hartree-Fock Exchange. *Chem. Phys.* **2009**, *356*, 98–109.

(13) Izsák, R.; Neese, F. An Overlap Fitted Chain of Spheres Exchange Method. *J. Chem. Phys.* **2011**, *135* (14), 144105.

(14) Aquilante, F.; Pedersen, T. B.; Lindh, R.; Roos, B. O.; Sánchez de Merás, A.; Koch, H. Accurate Ab Initio Density Fitting for Multiconfigurational Self-Consistent Field Methods.

(15) Malmqvist, P.-Å.; Roos, B. O. The CASSCF State Interaction Method. *Chem. Phys. Lett.* **1989**, *155* (2), 189–194.

(16) Singh, S. K.; Eng, J.; Atanasov, M.; Neese, F. Covalency and Chemical Bonding in Transition Metal Complexes: An Ab Initio Based Ligand Field Perspective. *Coord. Chem. Rev.* **2017**, *344*, 2–25.

(17) Atanasov, M.; Zadrozny, J. M.; Long, J. R.; Neese, F. A Theoretical Analysis of Chemical Bonding, Vibronic Coupling, and Magnetic Anisotropy in Linear Iron(II) Complexes with Single-Molecule Magnet Behavior. *Chem. Sci.* **2012**, *4* (1), 139–156.

(18) Angeli, C.; Cimiraglia, R.; Evangelisti, S.; Leininger, T.; Malrieu, J.-P. Introduction of N-Electron Valence States for Multireference Perturbation Theory. *J. Chem. Phys.* **2001**, *114* (23), 10252–10264.

(19) Angeli, C.; Cimiraglia, R.; Malrieu, J.-P. N-Electron Valence State Perturbation Theory: A Fast Implementation of the Strongly Contracted Variant. *Chem. Phys. Lett.* **2001**, *350* (3), 297–305.

(20) Angeli, C.; Cimiraglia, R.; Malrieu, J.-P. N-Electron Valence State Perturbation Theory: A Spinless Formulation and an Efficient Implementation of the Strongly Contracted and of the Partially Contracted Variants. *J. Chem. Phys.* **2002**, *117* (20), 9138–9153.
(21) Stoll, S.; Schweiger, A. EasySpin, a Comprehensive Software Package for Spectral Simulation and Analysis in EPR. *J. Magn. Reson.* **2006**, *178* (1), 42–55.